energies

MDPI

Article

An Accurate Model for Estimating H_2 Solubility in Pure Water and Aqueous NaCl Solutions

Zhiwei Zhu, Yuncheng Cao *, Zihan Zheng and Duofu Chen

Shanghai Engineering Research Center of Hadal Science and Technology, College of Marine Sciences, Shanghai Ocean University, Shanghai 201306, China; m18637601270@163.com (Z.Z.); zhzheng@shou.edu.cn (Z.Z.); dfchen@shou.edu.cn (D.C.)

* Correspondence: yccao@shou.edu.cn

Abstract: By employing a specific particle interaction theory and a high-precision equation of states for the liquid and vapor phases of H_2, respectively, a new H_2 solubility model in pure water and aqueous NaCl solutions is proposed in this study. The model established by fitting the experimental data of H_2 solubility can be used to estimate H_2 solubility in pure water at temperatures and pressures of 273.15–423.15 K and 0–1100 bar, respectively, and in salt solutions (NaCl concentration = 0–5 mol/kg) at temperatures and pressures of 273.15–373.15 K and 0–230 bar, respectively. By adopting the theory of liquid electrolyte solutions, the model can also be used to predict H_2 solubility in seawater without fitting the experimental data of a seawater system. Within or close to experimental data uncertainty, the mean absolute percentage error between the model-predicted and experimentally obtained H_2 solubilities was less than 1.14%.

Keywords: hydrogen; solubility; numerical simulation

check for updates

Citation: Zhu, Z.; Cao, Y.; Zheng, Z.; Chen, D. An Accurate Model for Estimating H_2 Solubility in Pure Water and Aqueous NaCl Solutions. *Energies* **2022**, *15*, 5021. https://doi.org/10.3390/en15145021

Academic Editor: Eugenio Meloni

Received: 13 May 2022
Accepted: 5 July 2022
Published: 9 July 2022

1. Introduction

Hydrogen (H_2) is an important natural gas because it is light, storable, and reactive [1]. H_2 is considered the best energy carrier for the efficient storage of renewable primary energy sources such as solar and wind energy [2]. On the one hand, the combustion of H_2 does not emit pollutants and greenhouse gases; the only combustion product is H_2O; on the other hand, H_2 has a high calorific value of ~140 MJ/kg [3]. H_2 is potentially suitable for large-scale geological storage in porous formations, saline aquifers, caverns, or depleted oil and gas reservoirs, all of which can provide significant storage capacity [4–6]. To assess the stability and safety of the long-term operation of hydrogen storage reservoirs and the efficiency of energy storage, one should study the solubility and volumetric properties of H_2 in gas−liquid systems for the migration of fluids and the alteration of minerals induced during storage [7]. Moreover, H_2 is abundantly present in nature. Hydrogen production can be divided into inorganic and organic geneses. Inorganic hydrogen is usually produced via earth degassing, water–rock reactions, and water radiolysis [8–10], whereas organic hydrogen is primarily produced via biogenesis and the thermal decomposition of organic matter [11,12]. Natural hydrogen is abundant in the formation areas of terrestrial volcanic rocks, large fault basins, marine serpentinized areas, and hydrothermal vents [9,13,14]. Hydrogen can be utilized as an electron donor in the reactions of photoautotrophic, photoheterotrophic, chemoautotrophic, and chemoheterotrophic organisms [15]. Most typically, autotrophic hydrogen bacteria consume hydrogen to produce life-sustaining methane, which explains the abundance of hydrogen-consuming organisms in submarine hydrothermal vents [16–18]. In studies on hydrogen-related biological activities or physicochemical processes, the hydrogen supply rate and hydrogen concentration in fluids must be determined. Moreover, H_2 solubility in a fluid largely determines the hydrogen transport rate and hydrogen concentration in the dissolved state.

Experiments using various solutions have yielded a large amount of H_2 solubility data at various temperatures and pressures. Additionally, H_2 solubility data have been accumulating since 1855. Using the pure physical absorption method, Bunsen [19] measured the absorption coefficients of H_2 in pure water at various temperatures (277.15–296.75 K) and atmospheric pressure. However, because H_2 shows low solubility in water at atmospheric pressure and the experimental conditions were limited, the measurement results were very similar. Using the same method, Wiebe and Gaddy [20] measured the absorption coefficients of hydrogen in pure water over a wide temperature range (273.15–373.15 K) and different pressures (25–1000 atm). They treated nitrogen impurities in the hydrogen so that gas composition was close to pure hydrogen and the influence of the water-vapor partial pressure on solubility was corrected. Chabab et al. [21] employed the static analysis method to measure H_2 solubility in pure water and aqueous NaCl solutions (1, 3, and 5 mol/kg) at different temperatures (323.18–372.76 K) and pressures (28.623–229.720 bar).

A model based on experimental data can be used to predict H_2 solubility in an unmeasured system. Jauregui-Haza et al. [22] studied H_2 solubility in water and organic solvents such as octene, toluene, and nonanal. They applied regular solution theory using the polar solvent factor correction method reported by Lemcoff [23]. Moreover, they derived the Henry constant of H_2 at temperatures of 353, 363, and 373 K. The H_2 solubility error in the aforementioned solvents was ~2.6%; however, the model was only applicable to pure aqueous solutions and the Henry constant of H_2 was not determined in aqueous NaCl solutions. Li et al. [7] considered the system pressure, temperature, and formation fluid salinity in an H_2 solubility model. Their model reproduced all available experimental data and accurately predicted H_2 solubility in formation fluids under a range of typical geological hydrogen storage conditions (273–373 K, 1–500 bar, and 0–5 mol/kg NaCl). Within or close to the experimental data uncertainty, H_2 solubility was predicted with a maximum relative error of 5% in pure water; however, the error increased to 15% in brine. Chabab et al. [21] estimated the H_2 solubility using a fast method based on a Setschenow-type relation [24], which predicted H_2 solubility in pure water and aqueous NaCl solutions with average deviations of 0.5% and 2%, respectively. This model was adapted to the temperature and pressure ranges of 273.15–373.15 K and 1–203 bar, respectively, in pure water, and 323.15–373.15 K and 10–230 bar, respectively, in aqueous NaCl solutions. However, in aqueous NaCl, the lower bound of this model was 323.15 K, which is unsuitable for studying H_2 solubility in nature. Torín-Ollarves and Trusler [25] proposed a simple model based on an analysis method for predicting H_2 solubility in aqueous solutions at temperatures and pressures of 273.15–423.15 K and 1–1010 bar, respectively. For reasons that defy a logical explanation, the prediction results of this model quite differed from those reported by Chabab et al. [21].

Duan et al. [26] established a solubility model of methane gas in aqueous solutions. Their model applies a specific theory of particle interactions for the liquid phase and a high-precision equation of state for the vapor phase. The methane solubility in both pure water and aqueous NaCl solutions was predicted for the temperature range of 273.15–523.15 K and the pressure range of 0–1600 bar. The error between the calculated and experimental data was ~7%. The parameters in this model were fitted to the experimental data and represented the interactions between substances. The values of different parameters were closely related, suggesting that the model is applicable to complex brines (e.g., $CaCl_2$, KCl, and seawater) using the approximation principle. The calculated results were consistent with the experimental data. Later, the solubilities of N_2, CO_2, C_2H_6, and O_2 in pure water to aqueous NaCl solutions were calculated using this model [27–31] and were also consistent with the experimental data. In conclusion, this model was widely applicable and can accurately calculate gas solubility in pure water and was easily employed in multiple ionic systems. Herein, we establish H_2 solubility models for the H_2 + H_2O system and the H_2 + H_2O + NaCl system, as well as for other ionized water systems that are applicable to a wide range of temperatures, pressures, and salinities. The gas-phase chemical potential of hydrogen was computed using the equation of state proposed by Peng and Robinson [32], whereas the liquid-phase chemical potential of hydrogen was defined using the theory

of liquid electrolyte solutions proposed by Pitzer [33]. The relevant parameters of this model were fitted to as many experimental data as possible. During comparison with experimental data, the model achieved high accuracy, thus providing a foundation for related marine geochemistry research.

2. H_2 Solubility Model

H_2 solubility in aqueous solutions was determined based on the balance between the chemical potentials of H_2 in the liquid and vapor phases. The potential can be expressed in terms of fugacity in the vapor phase (Equation (1)) and activity in the liquid phase (Equation (2)):

$$\begin{aligned} \mu^{l}_{H_2}(T,P,m) &= \mu^{l(0)}_{H_2}(T) + RT\ln a_{H_2}(T,P,m) \\ &= \mu^{l(0)}_{H_2}(T,P) + RT\ln m_{H_2} + RT\ln \gamma_{H_2}(T,P,m) \end{aligned} \tag{1}$$

$$\begin{aligned} \mu^{v}_{H_2}(T,P,y) &= \mu^{v(0)}_{H_2}(T) + RT\ln f_{H_2}(T,P,y) \\ &= \mu^{v(0)}_{H_2}(T) + RT\ln y_{H_2}P + RT\ln \varphi_{H_2}(T,P,y) \end{aligned} \tag{2}$$

where $\mu^{l(0)}_{H_2}$ and $\mu^{v(0)}_{H_2}$ represent the standard chemical potentials of H_2 in liquid and vapor phases, respectively. Here, $\mu^{l(0)}_{H_2}$ denotes the chemical potential in a hypothetical ideal solution of unit molality [34], and $\mu^{v(0)}_{H_2}$ denotes the chemical potential when the pressure of a hypothetical ideal gas is set to 1 bar.

At phase equilibrium $\mu^{l}_{H_2} = \mu^{v}_{H_2}$, subsequently, we obtain Equation (3).

$$\begin{aligned} \ln \frac{y_{H_2}P}{m_{H_2}} &= \frac{\mu^{l(0)}_{H_2}(T,P) - \mu^{v(0)}_{H_2}(T)}{RT} - \ln \varphi_{H_2}(T,P,y) \\ &\quad + \ln \gamma_{H_2}(T,P,m) \end{aligned} \tag{3}$$

In parameterization, reference value $\mu^{v(0)}_{H_2}$ can be set to 0 for convenience as only the difference between $\mu^{l(0)}_{H_2}$ and $\mu^{v(0)}_{H_2}$ is important. Since the vapor phase has low water content, the fugacity coefficient of H_2 in gaseous mixtures is approximate to that of pure H_2 in the studied region. Therefore, $\ln \varphi_{H_2}$ can be approximated from the equation of state of pure H_2 (refer to Appendix A) [32]. The mole fraction y_{H_2}. of H_2 in the gas is calculated as follows.

$$y_{H_2} = 1 - y_{H_2O} = \frac{P - P_{H_2O}}{P} \tag{4}$$

If the partial pressure P_{H_2O} of water in the vapor phase is approximated as the saturated pressure of pure water [26,28–31], $\frac{\mu^{l(0)}_{H_2}}{RT}$ and $\ln \gamma^{l}_{H_2}$ will contain errors of up to 5%. However, these errors can be largely canceled by parameterization. Herein, the mole fraction y_{H_2O} of water in the vapor phase is estimated using the following semiempirical equation:

$$y_{H_2O} = \frac{x_{H_2O}P^{S}_{H_2O}}{\varphi_{H_2O}P} e^{\frac{v^{l}_{H_2O}(P - P^{S}_{H_2O})}{RT}} \tag{5}$$

where x_{H_2O} represents the mole fraction of H_2O in the liquid phase, which is approximated as 1 and $1–2x_{NaCl}$ in the H_2 + H_2O and H_2 + H_2O + NaCl systems, respectively, when dissolved hydrogen is neglected. The saturation pressure $P^{S}_{H_2O}$ (in bar) of water was calculated using an empirical equation (refer to Appendix B). The molar volume $v^{l}_{H_2O}$ of water in the liquid phase was approximated to the saturated liquid-phase volume of water and was calculated using the equation proposed by Sun et al. [35]. The fugacity coefficient

φ_{H_2O} of water was calculated using the following equation, which is obtained by fitting the methane–water experimental data [30].

$$\varphi_{H_2O} = e^{a_1+a_2P+a_3P^2+a_4PT+\frac{a_5P}{T}+\frac{a_6P^2}{T}} \quad (6)$$

The values of $a_1 - a_6$ are listed in Table 1. The water content in the vapor phase can be calculated accurately using Equations (5) and (6). The results for different temperatures are plotted in Figure 1.

Table 1. Parameters of Equation (6) [30].

Parameters	Values
a_1	$-1.42006707 \times 10^{-2}$
a_2	$1.08369910 \times 10^{-2}$
a_3	$-1.59213160 \times 10^{-6}$
a_4	$-1.10804676 \times 10^{-5}$
a_5	-3.14287155×10
a_6	$1.06338095 \times 10^{-3}$

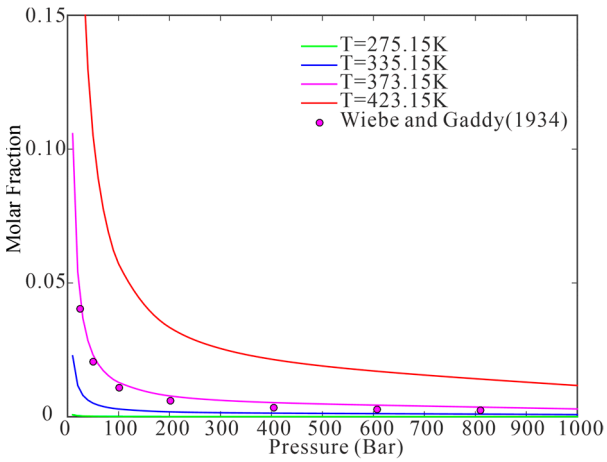

Figure 1. Pressure-dependent water content in the vapor phase as predicted using the model (The point reported by Wiebe and Gaddy [20]; The curves calculated using the proposed model).

$\ln \gamma_{H_2}$ is expressed as a virial expansion of excess Gibbs energy [33]:

$$\ln \gamma_{H_2} = \sum_c 2\lambda_{H_2-c} m_c + \sum_a 2\lambda_{H_2-a} m_a + \sum_c \sum_a \zeta_{H_2-c-a} m_c m_a \quad (7)$$

where λ and ζ represent the second-order and third-order interaction parameters, respectively. The subscripts c and a denote cations and anions, respectively. Substituting Equation (7) into Equation (3) yields the following.

$$\begin{aligned} \ln \frac{y_{H_2} P}{m_{H_2}} &= \frac{\mu_{H_2}^{l(0)}(T,P)}{RT} - \ln \varphi_{H_2}(T,P,y) \\ &+ \sum_c 2\lambda_{H_2-c} m_c + \sum_a 2\lambda_{H_2-a} m_a + \sum_c \sum_a \zeta_{H_2-c-a} m_c m_a \end{aligned} \quad (8)$$

Following Pitzer et al. [36], we selected the following equation for the T–P dependences of λ, ζ, and $\frac{\mu_{H_2}^{l(0)}}{RT}$.

$$Par(T,P) = c_1 + c_2 T + \frac{c_3}{T} + c_4 T^2 + c_5 P + \frac{c_6 P}{T^2} + \frac{c_7}{P} + c_8 \frac{T}{P} + c_9 \frac{T^2}{P} + c_{10} \frac{T^3}{P} \quad (9)$$

The basis of our model parameterization consists of Equations (8) and (9).

3. Results and Discussion

3.1. Review of H_2 Solubility Data

H_2 solubility in pure water and aqueous NaCl solutions was measured in a wide range of temperatures, pressures, and ionic strengths (Table 2). The remaining experimental data in pure water show good continuity and correlation, with the exception of some obvious deviations and relative dispersions. After including most of the experimental pure water data in the parameterization, the optimal ranges of temperatures and pressures for the H_2 + H_2O system in this model were determined to be 273.15–423.15 K and 0–1100 bar, respectively.

Alternatively, the experimental data of H_2 solubility in aqueous NaCl solutions showed poorer continuity and a narrower range than those in pure water. The measured values of H_2 solubility reported by Torín-Ollarves and Trusler [25] are obviously inconsistent with those reported by Chabab et al. [21]. These abnormal data were excluded, and the experimental data reported by Braun [37], Croizer and Yamamoto [38], and Chabab et al. [20] were selected for the parameterization. Finally, the solubility models for the H_2 + H_2O + NaCl system yielded temperature, pressure, and salinity ranges of 273.15–373.15 K, 0–230 bar, and 0–5 mol/kg, respectively.

The H_2 solubility has been measured in solutions other than aqueous NaCl solutions. For example, Braun [37] measured the H_2 solubility in 0.16–0.34 mol/kg $BaCl_2$ solution. Thomas et al. [32] and Gordon et al. [39] measured H_2 solubility in seawater with different salinities. Although the temperature ranges in these experiments were wide, the pressure was kept constant (1 atm). Because the aforementioned parameterization requires the combined effect of temperature, pressure, and salinity, these data were excluded from parameterization.

Table 2. Aqueous H_2 solubility measurements in the literature.

References	System	T (K)	P (bar)	N[a]
Bunsen [19]	Water	277.15–296.75	1^+	7
Timofejew [40]	Water	274.55–298.85	1^+	5
Bohr and Bock [41]	Water	273.15–373.15	1^+	48
Winkler [42]	Water	273.65–323.58	1^+	6
Braun [37]	Water	278.15–298.15	1^+	5
	0.21–4.03 m NaCl	278.15–298.15	1^+	5
	0.16–0.34 m $BaCl_2$	278.15–298.15	1^+	5
Ipatiew jun et al. [43]	Water	273.65–318.15	20.265–141.855	17
Wiebe and Gaddy [20]	Water	273.65–373.15	25.331–1013.250	40
Morrison and Billett. [44]	Water	285.65–345.65	1^+	12
Pray et al. [45]	Water	324.82–588.71	6.9–24.150	9
Ruetschi and Amlie [46]	Water	303.15	1^+	1
	0.0011–15.2% H_2SO_4	303.15	1^+	10
	0.0091–10.23% KOH	303.15	1^+	9
Shoor et al. [47]	Water	298.15-333.15	1^+	3
Longo et al. [48]	Water	310.15	1^+	1
Power and Stegall [49]	Water	310.15	1^+	1
Croizer and Yamamoto [38]	Water	274.60–302.47	1^+	42
	27.665–39.927‰ Seawater	274.65–303.49	1^+	180
	10.950–27.376‰ NaCl	274.03–301.51	1^+	10
Gordon et al. [39]	Water	273.29–302.40	1^+	7
	4.919–39.096‰ Seawater	272.80–302.41	1^+	32
Chou D Hary et al. [50]	Water	323.15–373.15	25.331–101.325	4
Alvarez et al. [51]	Water	318.90–636.10	6.78–284.5	26
Kling and Maurer [52]	Water	323.15–423.15	31.8–153.7	10
Jauregui-Haza et al. [22]	Water	353.15–373.15	1^+	3
Chabab et al. [21]	Water	323.18–372.73	29.272–121.706	6
	1–5 m NaCl	323.19–372.78	28.623–229.720	31
Torín-Ollarves and Trusler [25]	2.5 m NaCl	323.15–423.15	116.4–458.1	10

Note. 1^+ denotes that the partial pressure of hydrogen is 1 atm. N[a], number of measurements.

3.2. Construction and Validation of the Model

3.2.1. Determination of Model and Calculation of H_2 Solubility

To estimate H_2 solubility as a function of temperature, pressure, and salinity, we must determine parameters λ and ζ of Na^+ and Cl^- in the liquid phase and the standard chemical potential $\mu_{H_2}^{l(0)}$ in Equation (8). Because measurements can only be performed in electronically neutral solutions, one of the parameters must be assigned arbitrarily [53]. We set λ_{H_2-Cl} to zero and fitted the remaining parameters. First, $\frac{\mu_{H_2}^{l(0)}}{RT}$ was evaluated using the H_2 solubility data for pure water (92 related experimental data values), with a root mean square error of 1.62. Next, λ_{H_2-Na} and $\zeta_{H_2-Na-Cl}$ were evaluated simultaneously by the least-squares fitting of the solubility data for the aqueous NaCl solutions (41 related experimental data values), with a root mean square error of 1.42. The temperature- and pressure-dependent coefficients are listed in Table 3.

Table 3. Values of the interaction parameters in Equation (9).

Parameters	$\frac{\mu_{H_2}^{l(0)}(T)}{RT}$	λ_{H_2-c}	λ_{H_2-a}	ζ_{H_2-c-a}
c_1	4.18266086×10^{1}	$-7.68559552 \times 10^{0}$	0	$-1.44839161 \times 10^{-2}$
c_2	$-8.24713967 \times 10^{-2}$	$1.91233146 \times 10^{-2}$		
c_3	$-4.60318630 \times 10^{3}$	1.04890475×10^{3}		
c_4	$6.03537635 \times 10^{-5}$	$-1.52746819 \times 10^{-5}$		
c_5	$4.12979459 \times 10^{-4}$	$1.59803686 \times 10^{-4}$		
c_6	1.82081207×10^{1}	$-1.92667249 \times 10^{1}$		
c_7	3.73478602×10^{1}	$-4.75822792 \times 10^{1}$		
c_8	$-3.87633253 \times 10^{-1}$	$4.72712503 \times 10^{-1}$		
c_9	$1.34370747 \times 10^{-3}$	$-1.56750050 \times 10^{-3}$		
c_{10}	$-1.55621990 \times 10^{-6}$	$1.73272315 \times 10^{-6}$		

Substituting the parameters (Table 3) into Equation (8), we obtain the H_2 solubilities in pure water and aqueous NaCl solutions. The calculated solubilities in pure water and in 1, 3, and 5 mol/kg NaCl solutions are displayed in Tables 4–7.

Table 4. Calculated H_2 solubility (mol/kg) in pure water.

P (Bar)	T (K)					
	273.15	**303.15**	**333.15**	**363.15**	**393.15**	**423.15**
1	0.00095	0.00075	0.00070	0.00046	0	0
50	0.04700	0.03719	0.03560	0.03828	0.04370	0.05039
100	0.09248	0.07334	0.07030	0.07565	0.08657	0.10094
150	0.13675	0.10864	0.10426	0.11225	0.12856	0.15039
200	0.18006	0.14325	0.13758	0.14818	0.16980	0.19892
300	0.26458	0.21086	0.20269	0.21838	0.25031	0.29359
400	0.34720	0.27691	0.26622	0.28677	0.32863	0.38553
500	0.42864	0.34188	0.32857	0.35373	0.40514	0.47517
600	0.50942	0.40612	0.39002	0.41954	0.48013	0.56282
700	0.58990	0.46987	0.45080	0.48441	0.55384	0.64876
800	0.67033	0.53333	0.51105	0.54849	0.62644	0.73319
900	0.75091	0.59664	0.57091	0.61191	0.69806	0.81626
1000	0.83180	0.65989	0.63046	0.67477	0.76880	0.89811
1100	0.91310	0.72318	0.68979	0.73713	0.83875	0.97881

Table 5. Calculated H_2 solubility (mol/kg) in a 1 mol/kg NaCl solution.

P (Bar)	T (K)					
	273.15	**293.15**	**313.15**	**333.15**	**353.15**	**373.15**
1	0.00073	0.00063	0.00060	0.00055	0.00036	0
50	0.03002	0.02767	0.02700	0.02743	0.02858	0.03014
100	0.05953	0.05481	0.05341	0.05423	0.05663	0.06014
150	0.08884	0.08164	0.07942	0.08053	0.08406	0.08940
200	0.11810	0.10828	0.10512	0.10642	0.11097	0.11800
250	0.14743	0.13482	0.13059	0.13195	0.13741	0.14601

Table 6. Calculated H_2 solubility (mol/kg) in a 3 mol/kg NaCl solution.

P (Bar)	T (K)					
	273.15	**293.15**	**313.15**	**333.15**	**353.15**	**373.15**
1	0.00047	0.00043	0.00046	0.00036	0.00012	0
50	0.01336	0.01504	0.01654	0.01776	0.01857	0.01882
100	0.02691	0.03011	0.03288	0.03520	0.03702	0.03824
150	0.04091	0.04539	0.04921	0.05241	0.05502	0.05703
200	0.05542	0.06096	0.06559	0.06945	0.07264	0.07524
250	0.07053	0.07687	0.08206	0.08635	0.08992	0.09292

Table 7. Calculated H_2 solubility (mol/kg) in a 5 mol/kg NaCl solution.

P (Bar)	T (K)					
	273.15	**293.15**	**313.15**	**333.15**	**353.15**	**373.15**
1	0.00034	0.00033	0.00039	0.00027	0.00004	0
50	0.00668	0.00918	0.01137	0.01291	0.01355	0.01319
100	0.01366	0.01857	0.02273	0.02566	0.02718	0.02731
150	0.02115	0.02834	0.03424	0.03830	0.04044	0.04086
200	0.02920	0.03853	0.04595	0.05089	0.05340	0.05388
250	0.03789	0.04921	0.05790	0.06345	0.06608	0.06640

3.2.2. Model Validation

Figures 2 and 3 show a comparison of the experimental data with the results predicted using our model. The model adequately represented most of the experimental data, remaining within or close to the experimental uncertainty (~1.14%).

In the *T*–*P*–*m* range covered by our model, H_2 solubility increased with increasing pressure and decreased with increasing ionic strength. The temperature dependence of H_2 solubility was more drastic (Figure 4). H_2 solubility was slightly dependent on the temperature at low pressures (<200 bar) but decreased and then increased with increasing temperature at high pressures (>200 bar). The isobaric minimum solubility point was observed at ~320 K and 200 bar (Figure 4).

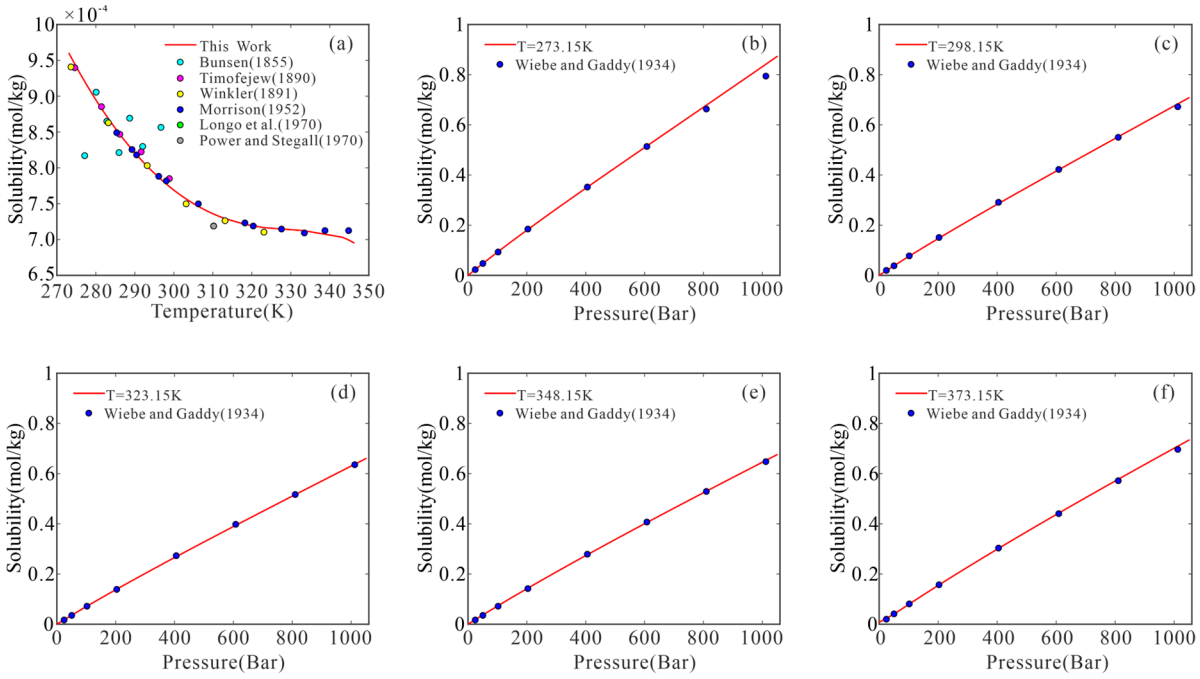

Figure 2. H_2 solubility versus pressure in pure water: model predictions (red lines) and experimental data (colored circles). ((**a**) The point reported by Bunsen [19], Timofejew [40], Winkler [42] Morrison [44], Longo et al. [48] and Power and Stegall [49]; (**b**–**f**) The point reported by Wiebe and Gaddy [20]; All the curves calculated using the proposed model).

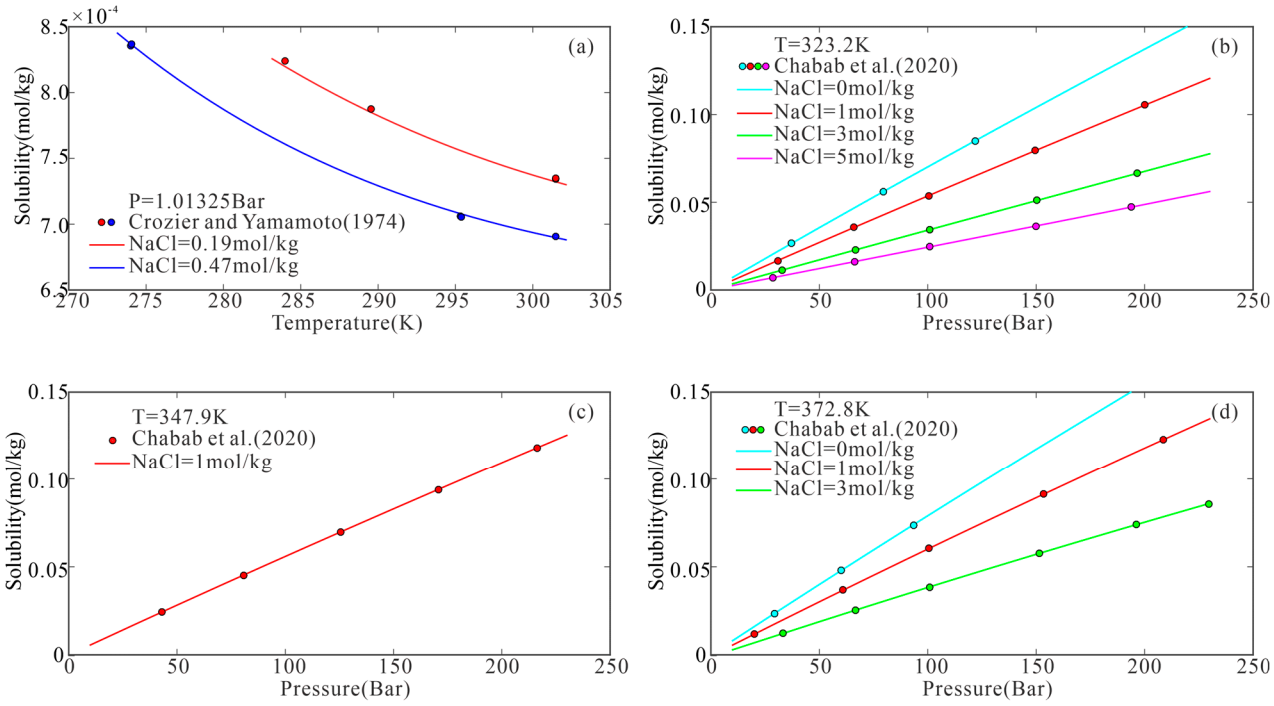

Figure 3. H_2 solubility versus pressure in aqueous NaCl solutions with different concentrations: model predictions (colored lines) and experimental data (colored circles). ((**a**) The point reported by Crozier and Yamamoto [38]; (**b**–**d**) The point reported by Chabab et al. [21]; All the curves calculated using the proposed model).

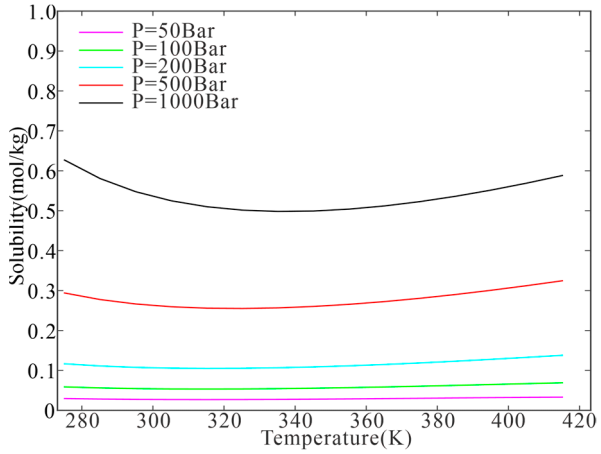

Figure 4. Isobaric minimum solubilities of H_2 in pure water.

The aforementioned solubility model may also be used to calculate the partial molar volume $\overline{V}_{H_2(l)}$, Henry's constant k_H, and the heat of solution $\triangle H^s_m$ of H_2 in aqueous NaCl solutions. At a given temperature, we can set P to 20 times of $P^S_{H_2O}$ for the calculation of Henry's constant. The functions are expressed using Equations (10)–(14).

$$\frac{\overline{V}_{H_2(l)}}{RT} = \frac{\partial}{\partial P}\left(\frac{\mu^{l(0)}}{RT}\right)_{T,m} + \left(\frac{\partial \ln \gamma_{H_2}}{\partial P}\right)_{T,m} \tag{10}$$

$$k_H(T) = \frac{y_{H_2}\varphi_{H_2}P}{x_{H_2}} e^{\frac{-\overline{V}_{H_2(l)}(P-P^s_{H_2O})}{RT}} \tag{11}$$

$$-\frac{\triangle H^s_m}{RT^2} = \frac{\partial}{\partial T}\left(\frac{\mu^{l(0)}}{RT}\right)_{P,m} + \left(\frac{\partial \ln \gamma_{H_2}}{\partial T}\right)_{P,m} \tag{12}$$

$$\left(\frac{\partial Par(T,P)}{\partial P}\right)_{T,m} = c_5 + \frac{c_6}{T^2} - \frac{c_7}{P^2} - \frac{c_8 T}{P^2} - \frac{c_9 T^2}{P^2} - \frac{c_{10} T^3}{P^2} \tag{13}$$

$$\left(\frac{\partial Par(T,P)}{\partial T}\right)_{P,m} = c_2 - \frac{c_3}{T^2} + 2c_4 T - 2\frac{c_6 P}{T^3} + \frac{c_8}{P} + 2\frac{c_9 T}{P} + 3\frac{c_{10} T^2}{P} \tag{14}$$

Tables 8 and 9 list the molar heat of the solution and Henry's constants of H_2 in water, respectively, obtained experimentally and calculated using our model. When the temperature was high, Henry's constants were closer only at higher pressures. There will still be small errors, but this is an acceptable range. Both sets of results demonstrated good agreement, affirming the reliability of the model from another perspective.

Table 8. Molar heat of solution of H_2 in water.

T (K)	P (Bar)	$-\Delta H^s_m$ (KJ/mol)
275.15	1	62.30
280.15	1	57.58
285.15	1	51.59
290.15	1	44.15
295.15	1	35.12
300.15	1	24.33
305.15	1	11.60

Table 9. Henry's constant (k_H) of H_2 in pure water (k_{H1} reported by Fernandez-Prini and Roberto [54]; k_{H2} calculated using the proposed model).

T (K)	$P^S_{H_2O}$ (Bar)	k_{H1}	k_{H2}
279.15	0.009	60,739.000	60,742.2020
290.15	0.019	67,113.000	65,737.9586
300.15	0.036	71,721.108	69,872.8408
350.15	0.420	77,317.000	71,095.8440
400.15	2.475	63,369.653	58,877.2595
423.15	4.751	54,667.000	53,262.5159

3.3. H_2 Solubility in Seawater: Extrapolation of the Model

A model developed using the specific interaction approach can be evaluated using binary and ternary data and then applied to more complicated systems [55]. Seawater often contains NaCl, KCl, $MgCl_2$, $CaCl_2$, and sulfate, as well as carbonate salts, although NaCl commonly dominates. As an example, Table 10 lists the main components in seawater with a salinity of 34.7‰. As data were limited, the model could only be directly fitted to the experimental results for the H_2–NaCl–H_2O system. We incorporated Ca^{2+}, K^+, Mg^{2+}, and $SO_4{}^{2-}$ into this model to tackle more complicated systems, utilizing the approximation suggested by Duan et al. [26].

Table 10. Main components of seawater with a salinity of 34.7‰.

Components	Concentration (mol/kg)
Cl^-	0.5405
Na^+	0.4645
K^+	0.01022
Ca^{2+}	0.4096
Mg^{2+}	0.0526
$SO_4{}^{2-}$	0.0279

The interaction parameters (λ and ζ) of ions with the same charge achieved approximately the same values. Within experimental accuracy, the interaction parameters of CH_4–bivalent cations were approximately double those of CH_4–monovalent cations at different temperatures and pressures. The interaction parameters of CH_4–anions were relatively small and therefore contributed little to the calculations. Hence, Duan et al. approximated all interaction parameters of CH_4–monovalent cations and CH_4–bivalent cations using λ_{CH_4-Na} and $2\lambda_{CH_4-Na}$, respectively [26]. By adopting the same approach, we approximated the H_2 solubility in seawater-type brines by setting the interaction parameters of H_2–monovalent cations and H_2–bivalent cations as λ_{H_2-Na} and $2\lambda_{H_2-Na}$, respectively. All ternary parameters were treated similarly. With this simplification, we achieved the following:

$$\begin{aligned} \ln m_{H_2} &= \ln y_{H_2} P + \ln \varphi_{H_2} - \frac{\mu^{l(0)}_{H_2}(T)}{RT} \\ &-2\lambda_{H_2-Na^+}\left(m_{Na^+} + m_{K^+} + 2m_{Ca^+} + 2m_{Mg^+}\right) \\ &-\zeta_{H_2-Na^+-Cl^-}\left(m_{Na^+} + m_{K^+} + 2m_{Ca^+} + 2m_{Mg^+}\right) \times \left(m_{Cl^-} + 2m_{SO_4^{2-}}\right) \\ &-2\lambda_{H_2-SO_4^{2-}} m_{SO_4^{2-}} \end{aligned} \quad (15)$$

where $\lambda_{H_2-SO_4^{2-}} = -3.572$. To check the accuracy of the approximation, we compared the calculated results of Equation (15) with the experimental data on the solubility of H_2 in seawater (Figure 5). The modeled results (p = 1 atm and T < 290 K) demonstrated excellent agreement with the experimental measurements.

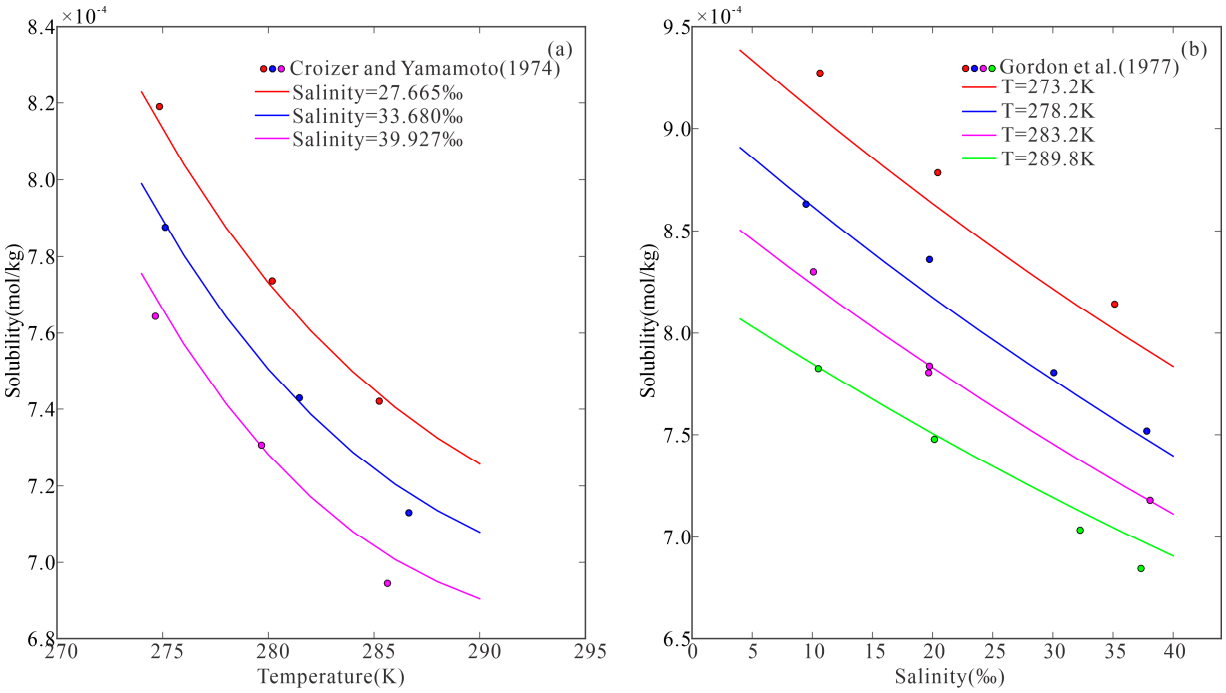

Figure 5. H_2 solubility in seawater versus temperature (**a**) and salinity (**b**). (Solid lines represent the modeled data, and the discrete symbols represent the experimental data [38,39]).

4. Conclusions

By applying a high precision equation of state to the vapor phase and the theory of liquid electrolyte solutions proposed by Pitzer to the liquid phase, we developed an accurate model of H_2 solubility in pure water and aqueous NaCl solutions. The results were within or close to the experimental uncertainty in pure water (273.15–423.15 K and 0–1100 bar) and aqueous NaCl solutions (273.15–373.15 K, 0–230 bar, and 0–5 mol/kg). After a simple extrapolation, the model predicted H_2 solubility in complex aqueous solutions such as seawater containing Na^+, K^+, Mg^{2+}, Ca^{2+}, Cl^-, and SO_4^{2-} with remarkable accuracy. The mean absolute percentage error between this model and experimentally obtained H_2 solubilities was less than 1.14%. The model can calculate hydrogen solubility not only in the subsea environments but also under several typical hydrogen geological storage conditions.

Author Contributions: Conceptualization, Z.Z. (Zhiwei Zhu); investigation, Z.Z. (Zhiwei Zhu); methodology, Z.Z. (Zhiwei Zhu). and Y.C.; software, Z.Z. (Zhiwei Zhu) and Y.C.; supervision, Y.C. and D.C.; validation, Z.Z. (Zhiwei Zhu); writing—original draft, Z.Z. (Zhiwei Zhu); writing—review and editing, Z.Z. (Zhiwei Zhu) and Z.Z. (Zihan Zheng) All authors have read and agreed to the published version of the manuscript.

Funding: This paper is financially supported by the National Natural Science Foundation of China (No. 91858208, No. 41776050, and No. 41776080).

Institutional Review Board Statement: Not applicable.

Informed Consent Statement: Not applicable.

Data Availability Statement: Not applicable.

Conflicts of Interest: The authors declare no conflict of interest.

Nomenclature

List of symbols	
T	Absolute temperature (K)
P	Total pressure (bar): $P = P_{H_2} + P_{H_2O}$
R	Universal gas constant (83.14 bar·cm^3/mol/K)
y_i	Mole fraction of component i in the vapor phase
x_i	Mole fraction of component i in the liquid phase
m_i	Molality of component i in the liquid phase (mol/kg)
$\overline{V}$	The partial molar volume(cm^3/mol)
Greek letters	
α	Activity
φ	Fugacity coefficient
γ	Activity coefficient
μ	Chemical potential
λ	Interaction parameter
ξ	Interaction parameter
Subscripts	
a	Anion
c	Cation
Superscripts	
v	Vapor
l	Liquid
(0)	Standard state

Appendix A

Peng et al. [27] calculated the fugacity coefficient of hydrogen using the equation of state.

$$P = \frac{RT}{\nu - b} - \frac{a(T)}{\nu(\nu + b) + b(\nu - b)}. \tag{A1}$$

By setting the following:

$$A = \frac{aP}{R^2T^2}; B = \frac{bP}{RT}; Z = \frac{Pv}{RT}, \tag{A2}$$

Equation (A1) can be rewritten as follows.

$$Z^3 - (1 - B)Z^2 + \left(A - 3B^2 - 2B\right)Z - \left(AB - B^2 - B^3\right) = 0. \tag{A3}$$

Here, R denotes the general gas constant (8.314 J/mol/K), and a can be regarded as a measure of the intermolecular attraction force; b is a constant related to the size of the gas molecules. Both a and b can be obtained using the critical properties of hydrogen at the critical point.

$$T_r = \frac{T}{T_c}; a(T_c) = 0.45724\frac{R^2T_c^2}{P_c}; b(T_c) = 0.07780\frac{RT_c}{P_c}; Z_c = 0.307 \tag{A4}$$

$$a(T) = a(T_c)\alpha(T_r, w); b(T) = b(T_c) \tag{A5}$$

$$\sqrt{\alpha(T_r, w)} = 1 + \kappa\left(1 - \sqrt{T_r}\right) \tag{A6}$$

$$\kappa = 0.37464 + 1.54226\omega - 0.26992\omega^2 \tag{A7}$$

The critical temperature T_c and critical pressure P_c of hydrogen were 33.2 K and 1.3×10^6 Pa, respectively, and the acentric factor was -0.216. First, a and b values in the critical state were determined from the state parameters of hydrogen using Equation (A4). Then, a and b values at other temperatures and pressures were calculated using

Equations (A5)–(A7). Finally, the fugacity coefficient of hydrogen was estimated using Equation (A8), which is derived from Equation (A1).

$$\ln \frac{f}{P} = Z - 1 - \ln(Z - B) - \frac{A}{2\sqrt{2}B} \ln\left(\frac{Z + 2.414B}{Z - 0.414B}\right). \quad \text{(A8)}$$

Appendix B

The pure water pressure was calculated using the following empirical model [28]:

$$P^S_{H_2O} = \left(\frac{P_c T}{T_c}\right)\left[1 + c_1(-t)^{1.9} + c_2 t + c_3 t^2 + c_4 t^3 + c_5 t^4\right], \quad \text{(A9)}$$

where

$$t = \frac{T - T_c}{T_c}, \quad \text{(A10)}$$

and T_c and P_c represent the critical temperature and critical pressure of water, respectively (T_c = 647.29 K and P_c = 220.85 bar). The values of parameters c_1–c_5 in Equation (A9) are listed in Table A1.

Table A1. Parameters of Equation (A9).

Parameters	Values
c_1	−38.640844
c_2	5.8948420
c_3	59.876516
c_4	26.654627
c_5	10.637097

References

1. International Energy Agency. *The Future of Hydrogen*; International Energy Agency: Osaka, Japan, 2019; Volume 3.
2. Sørensen, B. Energy and Resources: A plan is outlined according to which solar and wind energy would supply Denmark's needs by the year 2050. *Science* **1975**, *189*, 255–260. [CrossRef] [PubMed]
3. Garrels, R.M.; Christ, C.L. Solutions, Minerals and Equilibria. New York. *Mineral. Mag.* **1966**, *35*, 1024–1025.
4. Foh, S.; Novil, M.; Rockar, E.; Randolph, P. *Underground Hydrogen Storage. Final Report. [Salt Caverns, Excavated Caverns, Aquifers and Depleted Fields]*; Brookhaven National Lab.: New York, NY, USA, 1979.
5. Carden, P.; Paterson, L. Physical, chemical and energy aspects of underground hydrogen storage. *Int. J. Hydrogen Energy* **1979**, *4*, 559–569. [CrossRef]
6. Evans, D. *An Appraisal of Underground Gas Storage Technologies and Incidents, for the Development of Risk Assessment Methodology*; British Geological Survey: Nottingham, UK, 2007; Volume 1.
7. Li, D.; Beyer, C.; Bauer, S. A unified phase equilibrium model for hydrogen solubility and solution density. *Int. J. Hydrogen Energy* **2018**, *43*, 512–529. [CrossRef]
8. Goebel, E.D.; Coveney, R.M.; Angino, E.E.; Zeller, E.J.; Dreschhoff, G.M. Geology, Composition, Isotopes of Naturally Occurring Rich Gas from Wells near Junction City, Kans. *Oil Gas J.* **1984**, *82*, 215–222.
9. Coveney, R.M., Jr.; Goebel, E.D.; Zeller, E.J.; Dreschhoff, G.A.; Angino, E.E. Serpentinization and the Origin of Hydrogen Gas in Kansas1. *AAPG Bull.* **1987**, *71*, 39–48.
10. Klein, F.; Tarnas, J.D.; Bach, W. Abiotic Sources of Molecular Hydrogen on Earth. *Elements* **2020**, *16*, 19–24. [CrossRef]
11. Seewald, J.S. Organic–inorganic interactions in petroleum-producing sedimentary basins. *Nature* **2003**, *426*, 327–333. [CrossRef]
12. Piché-Choquette, S.; Constant, P. Molecular Hydrogen, a Neglected Key Driver of Soil Biogeochemical Processes. *Appl. Environ. Microbiol.* **2019**, *85*, e02418-18. [CrossRef]
13. Marty, B.; Gunnlaugsson, E.; Jambon, A.; Oskarsson, N.; Ozima, M.; Pineau, F.; Torssander, P. Gas Geochemistry of Geothermal Fluids, the Hengill Area, Southwest Rift Zone of Iceland. *Chem. Geol.* **1991**, *91*, 207–225. [CrossRef]
14. Petersen, J.; Zielinski, F.U.; Pape, T.; Seifert, R.; Moraru, C.; Amann, R.; Hourdez, S.; Girguis, P.; Wankel, S.D.; Barbe, V.; et al. Hydrogen is an energy source for hydrothermal vent symbioses. *Nature* **2011**, *476*, 176–180. [CrossRef] [PubMed]
15. Anderson, R.E.; Reveillaud, J.; Reddington, E.; Delmont, T.O.; Eren, A.M.; McDermott, J.M.; Seewald, J.S.; Huber, J.A. Genomic variation in microbial populations inhabiting the marine subseafloor at deep-sea hydrothermal vents. *Nat. Commun.* **2017**, *8*, 1114. [CrossRef] [PubMed]
16. Amend, J.P.; Shock, E.L. Energetics of Overall Metabolic Reactions of Thermophilic and Hyperthermophilic Archaea and Bacteria. *FEMS Microbiol. Rev.* **2001**, *25*, 175–243. [CrossRef] [PubMed]

17. Schlegel, H.G. Production, Modification, and Consumption of Atmospheric Trace Gases by Microorganisms. *Tellus* **2016**, *26*, 11–20.
18. Scheuermann, P.P.; Xing, Y.; Ding, K.; Seyfried, W.E. Experimental measurement of H2(aq) solubility in hydrothermal fluids: Application to the Piccard hydrothermal field, Mid-Cayman Rise. *Geochim. Cosmochim. Acta* **2020**, *283*, 22–39. [CrossRef]
19. Bunsen, R. Ueber Das Gesetz Der Gasabsorption. *Eur. J. Org. Chem.* **1855**, *93*, 1–50. [CrossRef]
20. Wiebe, R.; Gaddy, V.L. The Solubility of Hydrogen in Water at 0, 50, 75 and 100° from 25 to 1000 Atmospheres. *J. Am. Chem. Soc.* **1934**, *56*, 76–79. [CrossRef]
21. Chabab, S.; Theveneau, P.; Coquelet, C.; Corvisier, J.; Paricaud, P. Measurements and Predictive Models of High-Pressure H2 Solubility in Brine (H2o+Nacl) for Underground Hydrogen Storage Application. *Int. J. Hydrog. Energy* **2020**, *45*, 32206–32220. [CrossRef]
22. Jáuregui-Haza, U.J.; Pardillo-Fontdevila, E.J.; Wilhelm, A.M.; Delmas, H. Solubility of Hydrogen and Carbon Monoxide in Water and Some Organic Solvents. *Lat. Am. Appl. Res.* **2004**, *34*, 71–74.
23. Lemcoff, N. Liquid phase catalytic hydrogenation of acetone. *J. Catal.* **1977**, *46*, 356–364. [CrossRef]
24. Setschenow, J. Über Die Konstitution Der Salzlösungen Auf Grund Ihres Verhaltens Zu Kohlensäure. *Z. Für Phys. Chem.* **1889**, *4*, 117–225. [CrossRef]
25. Torín-Ollarves, G.A.; Trusler, J.M. Solubility of hydrogen in sodium chloride brine at high pressures. *Fluid Phase Equilibria* **2021**, *539*, 113025. [CrossRef]
26. Duan, Z.; Møller, N.; Greenberg, J.; Weare, J.H. The Prediction of Methane Solubility in Natural Waters to High Ionic Strength from 0 to 250 °C and from 0 to 1600 Bar. *Geochim. Cosmochim. Acta* **1992**, *56*, 1451–1460. [CrossRef]
27. Sun, R.; Hu, W.; Duan, Z. Prediction of Nitrogen Solubility in Pure Water and Aqueous Nacl Solutions up to High Temperature. *Solut. Chem.* **2001**, *30*, 561–573. [CrossRef]
28. Duan, Z.; Sun, R. An improved model calculating CO_2 solubility in pure water and aqueous NaCl solutions from 273 to 533 K and from 0 to 2000 bar. *Chem. Geol.* **2003**, *193*, 257–271. [CrossRef]
29. Mao, S.; Zhang, Z.; Hu, J.; Sun, R.; Duan, Z. An accurate model for calculating C2H6 solubility in pure water and aqueous NaCl solutions. *Fluid Phase Equilibria* **2005**, *238*, 77–86. [CrossRef]
30. Duan, Z.; Mao, S. A thermodynamic model for calculating methane solubility, density and gas phase composition of methane-bearing aqueous fluids from 273 to 523K and from 1 to 2000bar. *Geochim. Cosmochim. Acta* **2006**, *70*, 3369–3386. [CrossRef]
31. Geng, M.; Duan, Z. Prediction of oxygen solubility in pure water and brines up to high temperatures and pressures. *Geochim. Cosmochim. Acta* **2010**, *74*, 5631–5640. [CrossRef]
32. Peng, D.Y.; Robinson, D.B. A New Two-Constant Equation of State. *Ind. Eng. Chem. Fundam.* **1970**, *15*, 3069–3078. [CrossRef]
33. Pitzer, K.S. Thermodynamics of Electrolytes. I. Theoretical Basis and General Equations. *Phys. Chem.* **1973**, *77*, 268–277. [CrossRef]
34. Denbigh, K.G. *The Principles of Chemical Equilibrium: With Applications in Chemistry and Chemical Engineering*; Cambridge University Press: Cambridge, UK, 1981.
35. Sun, R.; Huang, Z.; Duan, Z. A new equation of state and Fortran 77 program to calculate vapor–liquid phase equilibria of CH4–H2O system at low temperatures. *Comput. Geosci.* **2003**, *29*, 1291–1299. [CrossRef]
36. Pitzer, K.S.; Peiper, J.C.; Busey, R.H. Thermodynamic Properties of Aqueous Sodium Chloride Solutions. *J. Phys. Chem. Ref. Data* **1984**, *13*, 1–102. [CrossRef]
37. Braun, L. Über Die Absorption Von Stickstoff Und Von Wasserstoff in Wässerigen Lösungen Verschieden Dissociierter Stoffe. *Z. Für Phys. Chem.* **1900**, *33*, 721–739. [CrossRef]
38. Crozier, T.E.; Yamamoto, S. Solubility of Hydrogen in Water, Sea Water, and Sodium Chloride Solutions. *J. Chem. Eng. Data* **1974**, *19*, 242–244. [CrossRef]
39. Gordon, L.I.; Cohen, Y.; Standley, D.R. The solubility of molecular hydrogen in seawater. *Deep Sea Res.* **1977**, *24*, 937–941. [CrossRef]
40. Timofejew, W. Über Die Absorption Von Wasserstoff Und Sauerstoff in Wasser Und Alkohol. *Z. Für Phys. Chem.* **1890**, *6*, 141–152. [CrossRef]
41. Bohr, C.; Bock, J. Bestimmung der Absorption einiger Gase in Wasser bei den Temperaturen zwischen 0 und 100°. *Ann. Phys.* **1891**, *280*, 318–343. [CrossRef]
42. Winkler, L.W. Die Löslichkeit Der Gase in Wasser. *Ber. Dtsch. Chem. Ges.* **1891**, *24*, 89–101. [CrossRef]
43. Ipatiew, W.W.; Drushina-Artemowitsch, S.I.; Tichomirow, W.I. Löslichkeit Des Wasserstoffs in Wasser Unter Druck. *Ber. Dtsch. Chem. Ges.* **1932**, *65*, 568–571. [CrossRef]
44. Morrison, T.J.; Billett, F. The Salting-out of Non-Electrolytes. Part Ii. The Effect of Variation in Non-Electrolyte. *J. Chem. Soc.* **1952**, *1952*, 3819–3822. [CrossRef]
45. Pray, H.A.; Schweickert, C.E.; Minnich, B.H. Solubility of Hydrogen, Oxygen, Nitrogen, and Helium in Water at Elevated Temperatures. *Ind. Eng. Chem.* **1952**, *44*, 1146–1151. [CrossRef]
46. Ruetschi, P.; Amlie, R.F. Solubility of Hydrogen in Potassium Hydroxide and Sulfuric Acid. Salting-out and Hydration. *J. Phys. Chem.* **1966**, *70*, 718–723. [CrossRef]
47. Shoor, S.K.; Walker, R.D.; Gubbins, K.E. Salting out of nonpolar gases in aqueous potassium hydroxide solutions. *J. Phys. Chem.* **1969**, *73*, 312–317. [CrossRef]

48. Longo, L.D.; Delivoria-Papadopoulos, M.; Power, G.G.; Hill, E.P.; Re, F. Diffusion equilibration of inert gases between maternal and fetal placental capillaires. *Am. J. Physiol. Content* **1970**, *219*, 561–569. [CrossRef]
49. Power, G.G.; Stegall, H. Solubility of gases in human red blood cell ghosts. *J. Appl. Physiol.* **1970**, *29*, 145–149. [CrossRef]
50. Choudhary, V.R.; Parande, M.G.; Brahme, P.H. Simple apparatus for measuring solubility of gases at high pressures. *Ind. Eng. Chem. Fundam.* **1982**, *21*, 472–474. [CrossRef]
51. Alvarez, J.; Crovetto, R.; Fernández-Prini, R. The Dissolution of N2 and of H2 in Water from Room Temperature to 640 K. *Ber. Der Bunsenges. Für Phys. Chem.* **1988**, *92*, 935–940. [CrossRef]
52. Kling, G.; Maurer, G. The solubility of hydrogen in water and in 2-aminoethanol at temperatures between 323 K and 423 K and pressures up to 16 MPa. *J. Chem. Thermodyn.* **1991**, *23*, 531–541. [CrossRef]
53. Harvie, C.E.; Møller, N.; Weare, J.H. The Prediction of Mineral Solubilities in Natural Waters: The Na-K-Mg-Ca-H-Cl-So4-Oh-Hco3-Co3-Co2-H2o System to High Ionic Strengths at 25 °C. *Geochim. Cosmochim. Acta* **1984**, *48*, 723–751. [CrossRef]
54. Fernández-Prini, R.; Alvarez, J.L.; Harvey, A.H. Henry's Constants and Vapor-Liquid Distribution Constants for Gaseous Solutes in H2o and D2o at High Temperatures. *J. Phys. Chem. Ref. Data* **2003**, *32*, 903–916. [CrossRef]
55. Weare, J.H. Models of Mineral Solubility in Concentrated Brines with Application to Field Observations. *Rev. Mineral. Geochem.* **1987**, *17*, 143–176.